Nucleic Acids Research, 2025, **53**, gkaf500
https://doi.org/10.1093/nar/gkaf500
Chemical Biology and Nucleic Acid Chemistry

Twisting tetraplex DNA: A strand dynamics regulating i-motif function in diverse molecular crowding environments

Shuntaro Takahashi[1,2,*], **Saptarshi Ghosh**[1], **Marko Trajkovski**[3], **Tatsuya Ohyama**[1], **Janez Plavec**[3,*], **Naoki Sugimoto**[1,*]

[1]FIBER (Frontier Institute for Biomolecular Engineering Research), Konan University, 7-1-20 Minatojima-Minamimachi, Chuo-ku, Kobe 650-0047, Japan
[2]FIRST (Graduate School of Frontiers of Innovative Research in Science and Technology), Konan University, 7-1-20 Minatojima-Minamimachi, Chuo-ku, Kobe 650-0047, Japan
[3]Slovenian NMR Centre, National Institute of Chemistry, Hajdrihova 19, SI-1000 Ljubljana, Slovenia

[*]To whom correspondence should be addressed. Email: shtakaha@konan-u.ac.jp
Correspondence may also be addressed to Janez Plavec. Email: janez.plavec@ki.si
Correspondence may also be addressed to Naoki Sugimoto. Email: sugimoto@konan-u.ac.jp

Abstract

Intercalated motif (i-motif) tetraplex DNA plays a crucial role in gene expression and diseases. However, due to the limited number of i-motif binding proteins in human cells, the chemical mechanisms regulating i-motifs within cell remain currently unknown. Thus, molecular environment should have a main factor to control i-motif formation and functions in cells. Here, we systematically investigated the stability and functions of i-motif DNAs by using various polyethylene glycols (PEGs) and oligoethylene glycols (OEGs) that mimicked diverse cellular crowding environments. We found that the human telomere i-motif was significantly stabilized by PEGs and OEGs having six or more ethylene glycol units, whereas it was destabilized by those having less than six units. As these stabilization effects coincided with the drastic changes in hypochromicity by i-motif helixes, we quantitatively validated these effects through changes in solution properties and by assessing the twisting of the tetraplex structure using nuclear magnetic resonance (NMR) and molecular dynamics simulations. Furthermore, cosolute-induced twisting dynamics controlled by different cosolutes changed the activation energy barrier of replication by a twofold magnitude along the i-motif-forming DNAs. Our findings indicate that regulatory mechanisms underlying the biological roles of i-motifs across different cellular phases may exist by molecular environments.

Graphical abstract

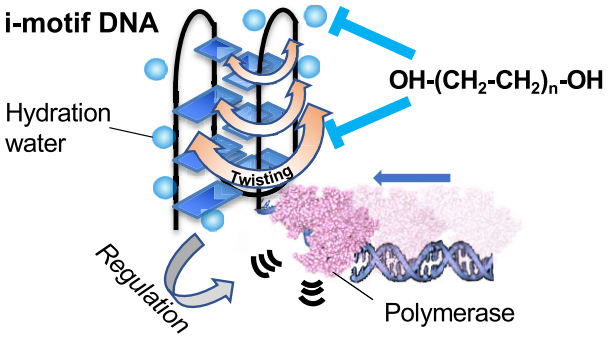

Introduction

Canonical duplex of nucleic acids (DNA and RNA) encodes and stores genetic information. DNA forms B-form duplex, which is different from A-form RNA duplex and thus conversely, non-canonical structures, such as Z-DNA/Z-RNA, triplexes, and tetraplexes, act as regulators of gene expression [1–3]. To induce and stabilize these non-canonical structures, specific binding proteins act as stabilizers for a particular motif in cells, regulating replication and transcription [4, 5]. Recently, another non-canonical structure, the intercalated motif (i-motif), which is a complementary sequence of G-quadruplex (G4), has been identified in human cells [6–8]. i-Motifs are formed by two intercalating parallel duplexes and stabilized by hemi-protonated cytosine–cytosine

Received: December 17, 2024. **Revised:** April 14, 2025. **Editorial Decision:** May 1, 2025. **Accepted:** June 18, 2025
© The Author(s) 2025. Published by Oxford University Press on behalf of Nucleic Acids Research.
This is an Open Access article distributed under the terms of the Creative Commons Attribution-NonCommercial License (https://creativecommons.org/licenses/by-nc/4.0/), which permits non-commercial re-use, distribution, and reproduction in any medium, provided the original work is properly cited. For commercial re-use, please contact reprints@oup.com for reprints and translation rights for reprints. All other permissions can be obtained through our RightsLink service via the Permissions link on the article page on our site—for further information please contact journals.permissions@oup.com.

Downloaded from https://academic.oup.com/nar/article/53/12/gkaf500/8178390 by Kemijski Institut user on 16 July 2025

base pairs ($C{\cdot}C^+$) found in cytosine-rich sequences prevalent in the telomere and promoter regions of human genes [9–11]. Their formation in cells is becoming a topic of research because potential i-motif sequences regulate replication and transcription, which can cause cancer [12–16]. Very recently, direct evidence between i-motif and diabetes were identified [17]. Moreover, i-motifs form interdependently against G4s during each cell-cycle step [8], which indicate a key role in aging. Recent *in vitro* and cellular studies have revealed that the structural stability of the i-motif determines its biological roles. For example, the stable formation of a specific i-motif allows interaction with G4s in the telomere via its loop region and regulates telomere elongation by telomerases [18]. Additionally, the stability of i-motifs relates to the spontaneous genomic DNA deletions [19]. Despite the biological significance of i-motifs, only a limited number of i-motif binding proteins have been reported in human cells [14, 20–23]. Moreover, almost no endogenous protein reported that specifically binds to and stabilises the i-motif structure has been identified in human cells [9]. Therefore, how cells control i-motif formations and their functions are not clearly understood.

The intracellular environment is a possible factor controlling i-motif formation and function, because i-motif stability is higher in cells than *in vitro* [7, 24]. The cellular environment contains highly concentrated cosolutes, including biomacromolecules and metabolites, reaching concentrations of up to 200–400 mg/ml [25]. This condition, termed molecular crowding, alters the physicochemical properties of the solution, such as water activity and dielectric constant, in addition to volume excluded by macromolecules [26]. Using soluble polymers as crowders *in vitro*, i-motif structures were stabilized, whereas canonical duplexes were destabilized [27–29]. These findings suggest that stable i-motif formation in cells is due to the specific physicochemical properties of the intracellular solution. Interestingly, i-motif formation in cells depends on the cell cycle [6], where intracellular conditions are spatiotemporally heterogeneous. These spatiotemporal changes in intracellular conditions may promote various functions in nucleic acids. For example, we previously identified that the topology of G4 could differ in the nucleus, nucleolus, and cytosol [30], indicating that G4 function should be regulated based on diverse intracellular conditions. In such distinct areas, nucleic acid stability also differed [31, 32]. Although i-motifs have no different topology, their folding can be more dynamic than that of G4s [22]. Therefore, diverse intracellular conditions potentially and diversely provide the necessary dynamics for the formation of i-motifs for various functions without being stabilized by proteins.

To understand the behaviour of the i-motif in cells, the classification of its biophysical and biochemical properties exhibited in a solution with defined physicochemical properties is required. To date, i-motif stability was thought to be chiefly due to the excluded volume effect, as larger molecular weight (MW) cosolutes such as polysaccharides and polyethylene glycol (PEG) tend to stabilize more than the smaller ones [33]. Conversely, acoustic and densimetric measurements have revealed that i-motif formation from the coil state is not accompanied by any volumetric change [34], suggesting that the excluded volume effect exerted by the cosolutes may not be the major factor affecting i-motif stability. Moreover, i-motif behaviour under solution conditions such as varied water activities and dielectric constants remains unclear. Therefore, a systematic analysis of the stability and function of i-motifs under different crowding conditions is necessary.

In this study, we investigated the effects of diverse molecular crowding on the structure and stability of i-motif DNA using spectroscopy and molecular simulation. To investigate the effect of molecular crowding on i-motif DNA, PEGs [30], and oligoethylene glycols (OEGs) as monodisperse EG polymers were used [33]. The thermodynamic stability revealed that the stability of the human telomere i-motif under the crowding conditions depended on the MW of the PEGs and OEGs and the pH of the solution. Compared with the thermodynamic stability ($-\Delta G^\circ_{37}$) of the i-motif without cosolutes ($-\Delta G^\circ_{37} = 2.9$ kcal mol^{-1}), PEGs with MWs $\geq$400 and OEGs having $\geq$ 6 units of ethylene glycol stabilized the i-motif ($-\Delta G^\circ_{37} > 3.6$ kcal mol^{-1}) at pH 5.0, whereas PEG200 and OEGs having <6 units were found to slightly destabilized the structure ($-\Delta G^\circ_{37} < 2.6$ kcal mol^{-1}). NMR and molecular dynamic (MD) simulations revealed twisting of the i-motif structure in the presence of PEGs with MWs $\geq$400. To consider an energetic parameter associated with the twisting, we reproduced i-motif stability in diverse crowding conditions based on the stability without cosolute. Furthermore, the kinetic analysis of the replication reaction indicated that i-motifs in the solution of larger PEGs more effectively stalled the replication reaction than those in the solution of smaller PEGs and OEGs. As i-motif formation in the cell nucleus undergoes dynamic changes influenced by cell cycles and cell types [6, 8, 35], our findings suggest that changes in molecular environments within the nucleus caused by cell cycles and cell types can induce variations in the stability and/or structure of i-motifs. This is due to the twisting of i-motifs, which regulates the resolution of i-motifs for smooth DNA replication. Therefore, the twisting of i-motifs under diverse crowding conditions could represent a chemical strategy aimed at maintaining genome integrity depending on the cell cycles and cell types.

Materials and methods

Materials

HPLC-grade oligonucleotides (Japan Bio Service, Saitama, Japan) were dissolved in MilliQ water and stored at −30°C before use. For the spectroscopic analyses, the i-motif sequences from the human telomere i-motif (hTelo iM: 5′-CCCTAACCCTAACCCTAACCCTAA-3′), Hif1a gene (cHif1a: 5′-CGCGCTCCCGCCCCCTCTCCCCTCCCCGCG-3′), ILPR gene (cILPR: 5′-CCCCACACCCCTGTCCCCACACCCCCGG-3′), and Bcl2 gene (cBcl2: 5′-CAGCCCCGCTCCCGCCCCCTTCCTCCCGCGCCCGCCCCTCGG-3′) were used. For the replication assay, the template DNAs containing each i-motif sequence shown above were used. Each template DNA was hybridized with the primer sequence labelled with fluorescein amidite (FAM) at the 5′ terminus and used for replication assays. All the sequences used in this study are shown in Supplementary Table S1. DNA concentration was determined by measuring the absorbance at 260 nm and 90°C using a Shimadzu 1700 spectrophotometer (Shimadzu, Kyoto, Japan) connected to a thermoprogrammer. PEGs with average MWs of 200, 400, 600, and 1000 (PEG200, PEG400, PEG600, and PEG1000) were purchased (Wako Pure Chemical Industries Ltd., Osaka, Japan). OEGs, which are tetraethylene glycol (EG_4), pentaethylene glycol (EG_5), hexaethylene glycol (EG_6), heptaethylene glycol (EG_7), octaethylene glycol (EG_8), nonaethylene glycol (EG_9), and decaethylene glycol (EG_{10})

Downloaded from https://academic.oup.com/nar/article/53/12/gkaf500/8178390 by Kemijski Institut user on 16 July 2025

were purchased (Tokyo Chemical Industry, Tokyo, Japan). The PEGs and OEGs were used without further purification. Na-phosphate (10 mM) or Na-acetate buffer (100 mM NaCl and 1 mM ethylenediaminetetraacetic acid (EDTA)) was prepared. Solutions containing PEGs or OEGs were prepared in these buffers, and the pH of the solutions was adjusted with HCl or NaOH. All other chemicals were purchased (Wako Pure Chemical Industries Ltd., Osaka, Japan) and used without further purification. The DNA solutions were dried *in vacuo* and dissolved in each buffer solution before the experiments.

Thermodynamic analysis

Ultraviolet (UV) absorption spectra were recorded using a Shimadzu 1700 spectrophotometer equipped with a thermoprogrammer. The concentration of DNA in all experiments was 10 μM, unless otherwise noted. UV melting curves were measured at 260 and 295 nm. Sample solutions were incubated at 90°C for 5 min and cooled to 0°C at a rate of 1.0°C min^{-1}. For melting, the sample solutions were incubated at 0°C for 5 min and heated to 90°C at a rate of 0.5°C min^{-1}. To calculate thermodynamic parameters (enthalpy change ΔH°, entropy change ΔS°, and free energy change at 37°C ΔG°_{37}) for i-motif formation and melting temperature (T_m), the melting curves were fitted to the theoretical equation for an intramolecular association [36] using KaleidaGraph Software [37]. Measurements of water activity and dielectric constants were performed as described previously [37, 38] and listed in Supplementary Table S2.

Circular dichroism spectroscopy

Circular dichroism (CD) experiments were performed using a JASCO J-1500 spectropolarimeter (JASCO, Tokyo, Japan) at 4°C. The CD spectra reported were the averages of at least three scans measured from 190 to 350 nm at a scan rate of 100 nm min^{-1}. Prior to the measurement, the sample was heated at 90°C, then cooled at a rate of −1°C min^{-1} to 4°C and maintained at 4°C for at least 1 h.

NMR spectroscopy

NMR experiments were performed using Bruker AVANCE NEO 800 MHz spectrometers with QCI (quadruple resonance NMR cryoprobe for triple resonance bio-NMR and fluorine applications) and TCI (proton-optimized triple resonance NMR) cryoprobes. NMR spectra were processed and analysed with Topspin 4.1.3 (Bruker, Germany) and NMRFAM-SPARKY software [39]. NMR experiments were performed on samples prepared in 90% H_2O + 10% ^2H_2O (v/v), 20- or 200-mM deuterated Na-acetate buffer (pH 4.0 or 5.0) with DNA concentrations ranging between 0.2 and 0.6 mM per strand. The DNA oligonucleotides for NMR experiments were synthesized on an H-8 synthesizer (K&A LaborGeräte) using standard phosphoramidite chemistry. NMR samples comprising the cosolutes were prepared in the presence of either 20 wt% deuterated ethylene glycol (Eurisotop) or 10 wt% deuterated polyethylene glycol 8000 (Polymer Source). ^{1}H NMR experiments were acquired with a spectral width of 24 ppm, 64 scans, 4 dummy scans, and a relaxation delay of 3 s. ^{1}H NMR chemical shifts were referenced with respect to the signal at δ 0.0 ppm, corresponding to sodium trimethylsilylpropanesulfonate (DSS). Assignment of the imino, amino, and methyl resonances relied on ^{15}N- and ^{13}C-edited HSQC experiments acquired on partially (8%) site-specifically ^{15}N- and ^{13}C-isotope labelled oligonucleotides. 2D NOESY spectra (mixing time = 300 ms) were acquired with 640 and 4096 complex data points in F1 and F2 dimensions, respectively. The excitation sculpting water suppression method was used in the 1D and 2D NMR experiments. The distances derived from the volume integrals of cross-peaks in 2D ^{1}H–^{1}H NOESY spectra (τ_m = 300 ms) using the isolated two-spin approximation were calibrated against a reference distance of 2.99 Å, corresponding to the intraresidual Me-H6 cross-peak of the T10 residue in a given 2D NOESY spectrum.

MD simulation

The initial structure of the i-motif DNA was obtained from the Protein Data Bank (PDB ID:1EL2 [40]). Since the 7th nucleotide in the structure was methylated and the 16th nucleotide was an uracil base, the 7th and 16th nucleotides were replaced with cytosine and thymine bases, respectively, using Discovery Studio Ver. 17.2.0. The proton state of the i-motif followed the initial structure. Using AmberTools, 15 sodium cations were placed around the phosphate groups of the i-motif to neutralize the system charge. For the i-motif, Amber ff99bsc0 was applied to nucleotides in the i-motif [41]. By contrast, there was no force field for nucleotides with protonated cytosine in Amber ff99bsc0. Thus, these molecules were applied to general AMBER force fields (GAFFs) [42, 43] with restrained electrostatic potential (RESP) charge calculated using the Gaussian 09 software [44]. These force fields were converted with the ACPYPE software [45] for Gromacs MDs package [46]. The size of the simulation box was set at 7.4 nm × 7.4 nm × 7.4 nm as a cube with a minimum distance of 2 nm between the i-motif and the box wall. The box was filled with TIP3P water molecules [47]. For simulating the system in the crowding conditions, since it is difficult to reproduce PEG molecules containing broadly distributed MWs, we used OEGs close to the average MW of each PEG as follows: EG_4, EG_9, EG_{13} and EG_{22} were used as PEG200, PEG400, PEG600, and PEG1000, respectively. These molecules were constructed using Discovery Studio and added to the system. The force fields of these molecules, as well as nucleotides with protonated cytosine, were employed by GAFF. To set the concentration of PEGs to 0.1 M, 24 PEG molecules were added to the system. Finally, 24 sodium cations and 24 chloride anions were randomly added to both the dilute and crowding conditions at a 0.1 M salt concentration.

Optimization and MDs simulations for these systems were performed using Gromacs Ver. 2020. After 10 000 steps of solvent optimization, 10 000 steps of system optimization were performed. The systems were heated to 298 K for a 100 ps canonical ensemble (NVT ensemble) by constraining the i-motif structure. Thereafter, the systems were equilibrated at 1 atm for 1 ns and sampled for 100 ns in an isothermal–isobaric ensemble (NPT ensemble). Simulations were performed three times for the system in a dilute solution in the presence of 0.1 M EG_4, EG_9, EG_{13}, and EG_{22}.

Calculation of the energetic contribution of excluded volume of the solution

The excluded volume depends on the volume of the nucleic acid structures as well as size of the cosolutes. In the presence of a significantly higher concentration of the cosolute compared with that of nucleic acid, $\Delta G^\circ_{37,ev\text{-}hTeloIM}$ was de-

Downloaded from https://academic.oup.com/nar/article/53/12/gkaf500/8178390 by Kemijski Institut user on 16 July 2025

termined using Equation (1):

$$\Delta G^{\circ}_{37,\text{ev-hTeloIM}} = RT \times \rho \times \Delta V \times C, \quad (1)$$

where R is the gas constant in kcal mol^{-1} K^{-1}, T is the temperature in kelvin (K), ρ is the density of water in kg L^{-1}, ΔV is the change in the excluded volume between the nucleic acid and the cosolute upon iM formation in L mol^{-1}, and C is the molal concentration of the cosolute in mol kg^{-1} [48]. ΔV for iM formation can be represented as Equation (2):

$$\Delta V = V_{\text{iM}} - V_{\text{ss}}, \quad (2)$$

where V_{iM} and V_{ss} are the volumes excluded by the iM and the single strands, respectively. V was determined from the following relation in Equation (3), considering iM as cylinder and cosolutes as polymeric chains [49];

$$V = N \times l^2 \times N_{\text{A}} \times k \times 10^{-27}, \quad (3)$$

where N is the monomer number present in the cosolute, l is the statistical segment length of the polymer in Å, N_{A} is Avogadro's number (6.022×10^{23} mol^{-1}), and k is a geometrical factor derived from the length and radius of the nucleic acid structure in Å. The factor 10^{-27} is used for the conversation of Å^3 to L.

Since the 24-mer hTelo iM can be considered as two 12-mer intercalated hairpins, the radius of the iM should be equal to the radius of a single hairpin structure, and the length should be equal to the length of a 12-mer hairpin, which is equal to the length of a 6-mer duplex. Using the parameters listed in Supplementary Table S3, we calculated V/N for iM-PEG using Equation (3) (Supplementary Table S3). From the calculated V/N values, the $\Delta V/N$ for iM-PEG was elucidated to be −0.44 L mol^{-1} using Equation 2. $\Delta G^{\circ}_{37,\text{ev-hTeloIM}}$ for the different PEGs and EGs were then calculated using Equation (1) and the values are listed in Supplementary Table S4.

DNA replication assay

The DNA replication assay was carried out at 37°C as reported [12]. Briefly, for reaction mixtures, FAM-labelled primers and each template DNA were annealed in the buffer used in the replication reaction: 1 μM annealed DNA, 1 μM Klenow Fragment DNA polymerase with 3′–>5′ exonuclease deficient (KF exo-), 250 μM dNTPs, 40 mM 2-(N-morpholino)ethanesulfonic acid (MES), 100 mM KCl, 8 mM $MgCl_2$, and 20 wt% PEG200, PEG400, PEG600, or PEG1000 adjusted at pH 6.0 were added as indicated. The reaction was initiated by adding KF exo- to the reaction mixture and stopped at the designated time by placing the aliquots into the stop solution containing EDTA and N,N-dimethylformamide (DMF). After the reaction was stopped, the reactants were separated through electrophoresis using polyacrylamide containing 7 M urea and analysed on the fluoroimager (FLA-5100, Fuji Film) to quantitatively detect the extended primer. The intensities of the bands were analysed using NIH ImageJ software. The amount of full-length product (P) was quantified by calculating the ratio of the intensity of full-length product bands to the intensity of all bands. The kinetic model was applied to the two-step sequential model was as follows:

$$P_0 \xrightarrow{k_{\text{s}}} P_{\text{s}} \xrightarrow{k_{\text{f}}} P_{\text{f}},$$

$$\frac{\text{d}[P_0]}{\text{d}t} = -k_{\text{s}}[P_0],$$

$$\frac{\text{d}[P_{\text{s}}]}{\text{d}t} = k_{\text{s}}[P_0] - k_{\text{f}}[P_{\text{s}}],$$

$$\frac{\text{d}[P_{\text{f}}]}{\text{d}t} = k_{\text{f}}[P_{\text{s}}],$$

where P_0 is the starting state of the reaction; P_{s} is the state immediately after the stall is resolved; P_{f} state after replication of the full-length product is completed; k_{s} (min^{-1}), rate constant from the start of the reaction till the stall is resolved; and k_{f} (min^{-1}), rate constant from the resolution of the stall to the complete synthesis of the full-length product. Stalling before i-motif unfolding is the rate determining first step. The second step is replication progress after i-motif unfolding, which is faster than the unfolding itself [12]. Rate constants were evaluated by global fit using Dynafit (Biokin) to solve the above equations through numerical analyses.

Results and discussion

Thermodynamic stability of hTelo iM in the presence of PEGs and OEGs

We used the i-motif forming sequence d(C_3TA_2)$_4$ termed hTelo iM from human telomeres (Supplementary Table S1) as a structural model, because information on the tertiary structure of this i-motif structure is available [40]. To investigate the effect of molecular crowding on stability, we performed UV melting assays of hTelo iM in the presence of PEGs and OEGs with different MWs and obtained thermodynamic parameters for hTelo iM formation (ΔH°, ΔS°, and ΔG°_{37}) and melting temperature (T_{m}). At pH 5.0, we measured the hyperchromicity at 260 nm, originating from the dissociation of the C·C$^+$ base pair stabilized by the induced dipole moment. Melting profiles indicated that, compared to the stability in the absence of PEGs, PEG200 had a marginal effect on the stabilization of hTelo iM, whereas PEGs with an average MW of ≥400 stabilized the hTelo iM structure (Supplementary Fig. S1A). The thermodynamic parameters for hTelo iM in solutions with different PEGs were derived by fitting the melting curves and are listed in Table 1. As shown in Supplementary Fig. S1A, Table 1 reflects that hTelo iM stability at 37°C ($-\Delta G^{\circ}_{37}$) slightly decreased in the presence of PEG200, with values of $-\Delta G^{\circ}_{37}$ being 2.9 kcal mol^{-1} in the absence of PEGs and 2.6 kcal mol^{-1} in the presence of 20 wt% PEG200, respectively. By contrast, $-\Delta G^{\circ}_{37}$ values of hTelo iM increased significantly in the presence of 20 wt% PEG400, PEG600, and PEG1000 by 0.7, 0.9, and 0.9 kcal mol^{-1}, respectively. The

Table 1. Thermodynamic parameters of hTelo iM[a]

Cosolute[b]	T_{m} (°C)	ΔH° (kcal mol^{-1})	$T\Delta S^{\circ}$ (kcal mol^{-1})	$-\Delta G^{\circ}_{37}$ (kcal mol^{-1})
Without PEG	53.9 ± 0.7	−58.8 ± 4.7	−55.9 ± 4.4	2.9 ± 0.3
PEG200	52.6 ± 1.3	−54.3 ± 10.2	−51.7 ± 9.5	2.6 ± 0.7
PEG400	64.9 ± 1.2	−43.9 ± 2.8	−40.3 ± 2.5	3.6 ± 0.4
PEG600	64.0 ± 1.2	−48.6 ± 6.6	−44.8 ± 6.1	3.8 ± 0.5
PEG1000	63.9 ± 1.7	−47.5 ± 6.0	−43.7 ± 5.8	3.8 ± 0.3
EG_4	59.9 ± 2.5	−41.3 ± 4.8	−38.5 ± 4.5	2.8 ± 0.4
EG_5	55.1 ± 2.6	−46.5 ± 6.8	−43.9 ± 6.8	2.5 ± 0.2
EG_6	62.7 ± 1.7	−44.8 ± 5.0	−41.4 ± 4.5	3.4 ± 0.5
EG_7	62.4 ± 0.4	−43.2 ± 3.3	−39.9 ± 3.0	3.3 ± 0.3
EG_8	64.8 ± 1.6	−42.9 ± 11.7	−39.4 ± 10.8	3.5 ± 0.8
EG_9	66.1 ± 1.9	−49.6 ± 10.9	−45.4 ± 9.8	4.3 ± 1.1
EG_{10}	60.4 ± 3.8	−48.0 ± 5.2	−44.7 ± 5.4	3.3 ± 0.3

[a]The buffer condition was 10 mM sodium phosphate buffer containing 100 mM NaCl and 1 mM EDTA (pH 5.0).
[b]The concentration of cosolute was 20 wt%.

Downloaded from https://academic.oup.com/nar/article/53/12/gkaf500/8178390 by Kemijski Institut user on 16 July 2025

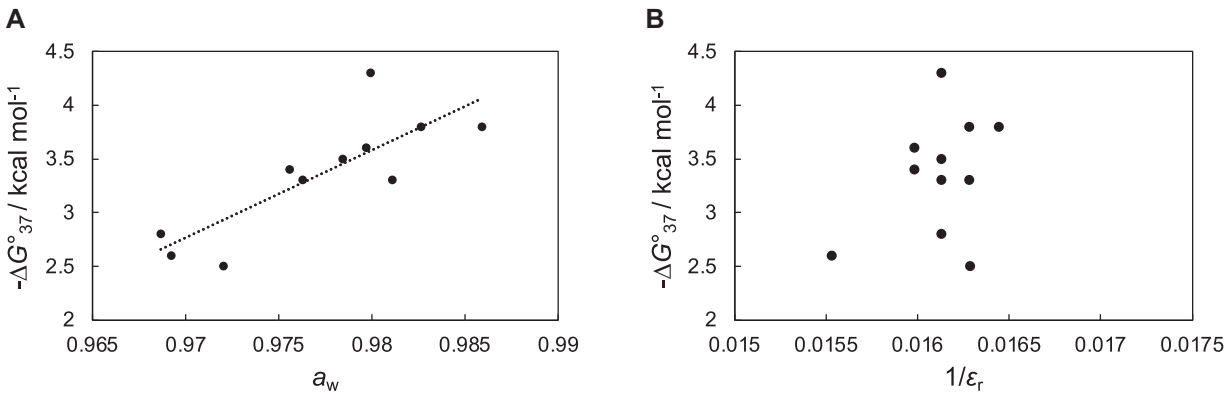

Figure 1. Plot of $-\Delta G^{\circ}_{37}$ of hTelo iM against (**A**) water activity (a_w) and (**B**) dielectric constant (ε_r) of the cosolute solutions. Each solution was buffered with 10 mM sodium phosphate buffer containing 100 mM NaCl and 1 mM EDTA (pH 5.0). The cosolute concentration was 20 wt% at 37°C.

drastic change between the effects of PEG200 and PEG400 on the stability of hTelo iM was confirmed in the presence of 20 wt% monodisperse ethylene glycol (EG) polymer OEG. Table 1 shows that the $-\Delta G^{\circ}_{37}$ values of hTelo iM in EG_4 and EG_5 were similar to the diluted solution but they were markedly increased in EG_6 (MW = 282) and larger. The thermodynamic parameters in all these cases (Table 1) show that i-motif stabilization is dominated by a favourable enthalpic contribution.

We also tracked the absorbance at 295 nm that showed hypochromicity for the i-motif as the signature of non-duplex structures [50]. Interestingly, we found that the magnitude of hypochromicity decreased with increasing MW at 20 wt% PEGs with a MW of >400 or EG_6 (Supplementary Fig. S1). As the hypochromicity depends on the stacking of the bases [51], the i-motif structure could be differently affected by each PEG molecule. However, the CD spectra of hTelo iM showed signatures of typical i-motif structures [52] without changes in the presence of PEGs (Supplementary Fig. S2A), suggesting that the global conformation of hTelo iM remained unaffected in the presence of PEGs. Therefore, the decrease in hypochromicity at 295 nm was due to changes in the local geometry of the tetraplex configuration. The decrease in hypochromicity was obvious for PEG400 and PEG1000 (Supplementary Fig. S1B).

The stability of hTelo iMs in the presence of PEG400 and PEG1000 was relatively high. To test the relation between the hypochromicity and the stability of the i-motif, the UV melting of hTelo iM was conducted in more and less stable conditions by varying the pH. At pH 4.0, the i-motif structure becomes more stable than that at pH 5.0, because the pK_a of cytosine is 4.3. The UV absorbance changes at 295 nm showed hyperchromicity in all the cases with any MW of 20 wt% PEGs (Supplementary Fig. S3). By contrast, in the less stable condition at pH 6.0, due to reduction of protonation of cytosines, the hypochromicity at 295 nm with the increasing MW of the PEGs at pH 6.0 was a lot less than that of the solutions at pH 5.0 (Supplementary Fig. S4). Therefore, PEGs may alter the configuration of the stacked $C{\cdot}C^+$ base pairs of hTelo iM and stabilise the structure, similar to the stabilizing effect of acidic conditions on i-motif stability.

Analysis of physicochemical properties affecting hTelo iM stability

The results above indicated that the difference in the stability and structure of hTelo iM between PEG200 and PEG400 was due to changes in some physicochemical properties of the solution related to their MW such as water activity, the dielectric constant, and the excluded volume effect [27, 53]. In particular, the change in the water activity of the cosolute solutions depends on their chemical nature and MW [54]. We plotted $-\Delta G^{\circ}_{37}$ of hTelo iM measured in the presence of 20 wt% of different OEGs and PEGs against their respective water activity (a_w) values (Supplementary Table S2 and Fig. 1A). The plot showed a positive correlation between i-motif stability and water activity. This trend was similar to the cases of duplexes [54], which indicated that the i-motif formation was accompanied by specific hydration of the formed structure [34]. The observation is also consistent with the previous report [55], in which the stability of the c-MYC i-motif was studied in the presence of different cosolutes. The concentration dependency of PEGs indicates that the stability of hTelo iM increased with increasing concentration of PEGs, except for PEG200, in which stability remained almost unaffected up to 20 wt% cosolute concentration and then slightly destabilized at 40 wt% (Supplementary Fig. S5). As for the dielectric constant (ε_r), no specific trend in the i-motif stability against $1/\varepsilon_r$ values was observed because $1/\varepsilon_r$ values did not vary in solutions containing each cosolute (Supplementary Fig. S4 and Fig. 1B). In a previous report, the stability of the i-motif did not change with changing salt concentrations [56], suggesting that the dipole moment of the base pairs and the electric repulsion of the phosphate backbones are not significantly affected by changes in dielectric constants. Regarding the exclude volume effect, the formation of the DNA structure should be facilitated by larger cosolutes. Thus, the excluded volume effect by cosolutes contributed to the stabilization of hTelo iM with PEG400 and larger cosolutes. Therefore, the analysis of the physicochemical properties of the i-motif stability suggested that water activity played a crucial role in the destabilization of solutions containing relatively small cosolutes such as PEG200 and stabilization of solutions containing larger cosolutes. However, based on UV spectroscopic data, there can be a specific mechanism that causes certain configuration changes in the i-motif structure via a larger cosolute, which stabilizes

Downloaded from https://academic.oup.com/nar/article/53/12/gkaf500/8178390 by Kemijski Institut user on 16 July 2025

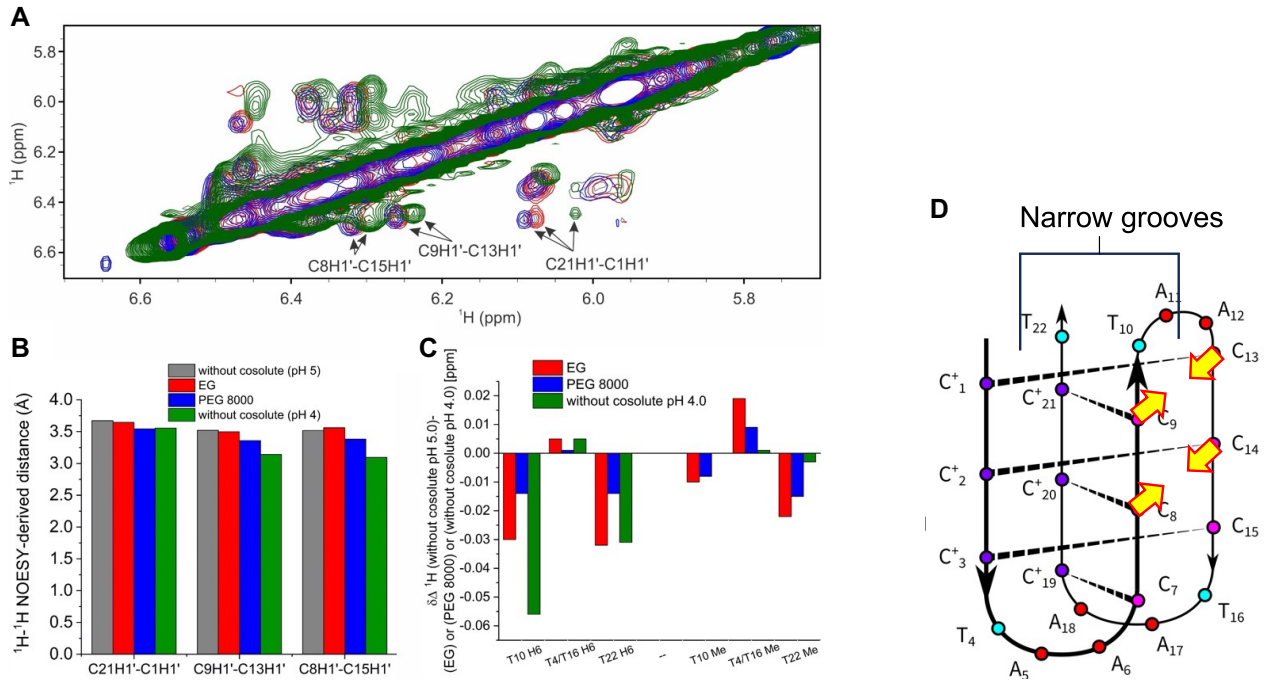

Figure 2. NMR spectroscopy for i-motif twisting. (**A**) Overlay of NOESY NMR spectra of hTelo 22 iM acquired at 25°C without cosolutes pH 5.0 (grey), in the presence of 20 wt% EG at pH 5.0 (red), in the presence of 10 wt% PEG 8000 at pH 5.0 (blue) and without cosolutes at pH 4.0 (green). (**B**) Distances between anomeric H1′ protons C1 and C21, C9 and C13, and C8 and C15 assessed from NOESY spectra. (**C**) ^{1}H NMR chemical shift differences of methyl (Me) and aromatic (H6) protons of thymine residues of hTelo 22 iM in the presence of 20 wt% EG, 10 wt% PEG 8000 and without cosolute at pH 4.0 with respect to without cosolutes at pH 5.0 deduced from the NMR spectra acquired at 25°C. (**D**) Schematic illustration of the static structural changes of narrow grooves suggested by NMR. Yellow arrows are images of the structural changes of the strands induced by PEGs.

i-motif DNA (Supplementary Fig. S1). This required further structural analyses at the atomic level to reveal the structural dynamics of i-motifs in PEGs.

Structural analysis of i-motif configuration by NMR

^{1}H NMR spectra of iM adopted by d($(C_3TA_2)_3C_3T$) named hTelo22 acquired from 10 to 35°C in the absence of cosolutes (Supplementary Fig. S6A) and the presence of 20 wt% EG (Supplementary Fig. S6B) or 10 wt% PEG8000 (Supplementary Fig. S6C) showed three intense and several broad imino signals in the region between δ 15.3 and 15.8 ppm. The analysis of other spectral regions including the aromatic one between δ 7.4 and 8.5 ppm (Supplementary Fig. S6A–C) indicated that hTelo22 adopted iM with similar features regardless on the presence of cosolutes. The comparison of integral values of ^{1}H NMR aromatic signals of single-stranded species and iM showed that iM was destabilized with EG and stabilized with PEG8000 as expected from UV melting (Supplementary Fig. S6D). The comparative analysis of structural details of iM adopted by hTelo22 relied on unambiguous assignment of the ^{1}H NMR imino (Supplementary Fig. S7) and amino (Supplementary Fig. S8) signals corresponding to C·C$^+$ base pairs, achieved with the use of ^{15}N-edited HSQC spectra acquired on a series of oligonucleotides prepared by incorporating partially ^{15}N-isotope labelled residue at individual positions (Supplementary Figs S7A–E and S8A). The NMR data in the absence and presence of EG and PEG8000 were consistent with hTelo22 adopting i-motif, in which C2·C14$^+$, C3·C15$^+$, and C8·C20$^+$ base pairs were buried within the core of the structure. The structure(s) exhibited additional C·C$^+$ base pairs, which were transiently formed as inferred from the corresponding broad imino ^{1}H NMR signals. In particular, up to four cross-peaks were observed in the ^{15}N-HSQC spectra of hTelo22 iM carrying a single ^{15}N-isotope labelled position. These data were in line with local structural variations that promote exchange of imino protons with the bulk solution for the cytosine residues beside the core of the structure. Further comparative analysis of i-motif adopted by hTelo22 iM in different conditions included comparison of NOE interactions that reflected the distances between pairs of proximal protons. Among the few non-overlapped NOESY cross-peaks interactions of anomeric protons of C1 and C21, C9 and C13, and C8 and C15 (Fig. 2A) reflected on the widths of the narrow grooves between C7–C9 and C13–C15 on one side and C1–C3 and C19–C21 on the other side of the i-motif structure. However, the observed differences between the NOE-derived widths of the narrow grooves at 25°C were within the margins of experimental error margin (Fig. 2B), consistent with EG and PEG8000 insignificantly affecting the i-motif structure. This was further corroborated through the observation of only minor, i.e. $\Delta\delta$ <0.03 ppm, EG- and PEG8000-induced perturbations in the thymine's aromatic H6 and methyl group ^{1}H NMR chemical shifts (Fig. 2C). Thus, considering the common folding topology under all three conditions, the cosolutes-related variations in the thermodynamic stability of i-motif adopted by hTelo22 iM shown above may originate from conformation fluctuations at microseconds or at a faster time scale on the NMR chemical shift.

To investigate the relation between the hyperchromic effect observed in the UV melting experiments and the structure of i-motifs, NMR characterization of hTelo22 iM was conducted in an aqueous solution in the absence of

Downloaded from https://academic.oup.com/nar/article/53/12/gkaf500/8178390 by Kemijski Institut user on 16 July 2025

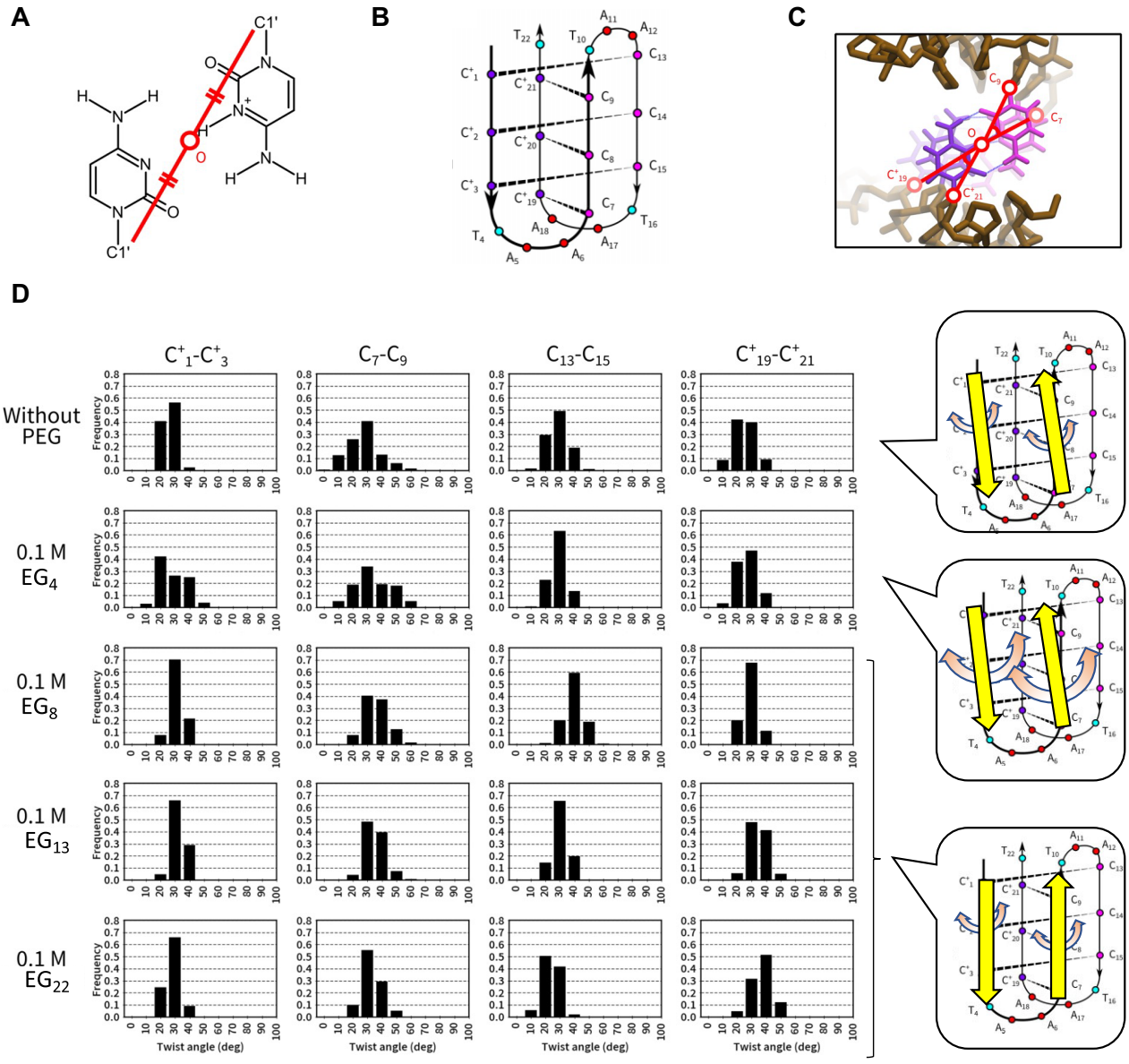

Figure 3. MD simulation of human telomere i-motif in the presence of different PEGs. (**A**) Schematic illustration of the central axis as the axis connecting the midpoints between the C1′ atoms. (**B**) Schematic structure of i-motif used for the simulation. (**C**) Image of the twist angle. C_7–C_9 and C^+_{19}–C^+_{21} are shown as examples. (**D**) Distribution of twist angles of hTelo iM and schematic illustrations of structural dynamics of i-motif structure. Arrows are images of the strand fluctuations and the polarity of the strands, respectively.

cosolute at 25°C and pH 4.0 (Supplementary Fig. S3). In particular, the analysis of NOE cross-peaks-derived distances between the pairs of anomeric protons C1H1'–C21H1', C9H1'–C13H1', and C8H1'–C15H1' (Fig. 2A and B) indicated that the widths of the narrow groove between C7–C9 and C13–C15 segments in hTelo22 iM became narrower upon lowering pH from 5.0 to 4.0 in the absence of cosolutes. Additionally, the analysis of thymine residues' ^{1}H NMR chemical shift perturbations under different conditions studied (Fig. 2C) showed minor changes, except for T10 H6 at pH 4.0. These results confirmed the above interpretation regarding the low pH-induced structural modulation of the i-motif adopted by hTelo22 iM at the C7–C9 and C13–C15 segments bridged by the T10-A11-A12 loop. As the minor grooves in the i-motif are already extremely narrow, with inter-strand sugars in close contact, this result suggest that the strands of hTelo22 iM undergo twisting and change the minor groove structure at the condition that showed hyperchromicity (Fig. 2D).

Twisting of i-motif configuration elucidated by MDs simulation

NMR was limited to measurements in the presence of EG and PEG8000, providing indirect information regarding the structural dynamics of hTelo iM. Thus, MDs simulations were carried out to study the structural changes and dynamics at the atomic level under different PEG and OEG conditions. We used the NMR structure of hTelo22 iM [40] as the initial structure of MD simulations under 100 mM Na^+ condition in the absence and presence of PEGs. As a system with the presence of OEGs, 0.1 M of EG_4, EG_9, EG_{13}, and EG_{22} closely

Downloaded from https://academic.oup.com/nar/article/53/12/gkaf500/8178390 by Kemijski Institut user on 16 July 2025

corresponding to the average MW of PEG200, PEG400, PEG600, and PEG1000, respectively, were added into solution. We used equilibrated simulation data obtained after 50–100 ns simulation of three different runs, as suggested by the root mean square deviation data for coordinates of all atoms on riboses and phosphates on the backbone of the i-motif, except for hydrogen atoms (Supplementary Fig. S9). First, we analysed the distance between the protons of C1 and C21, C9 and C13, and C8 and C15, similar to the NMR analysis. The average distances in the presence of each OEG did not show any changes dependent on the size of OEGs in the simulated structures indicated by NMR data (Supplementary Fig. S10). The relatively longer distance in the C21H1′-C1H1′ may be due to the simulation biases because these terminal base pairs are flexible and fluctuate. We also analysed the interphosphate distance within the minor groove of the i-motif and observed that OEGs did not decrease this distance compared to that in the condition without cosolute (Supplementary Fig. S11). To find the global structural changes in the i-motifs that could not be detected by NMR, we analysed the twist angles of the backbone of the i-motif helix to study the twisting of the structure. This was because the UV data suggested changes in the polarity of the dipole moment of C·C$^+$ base pairs. We defined the central axis as the axis connecting the midpoints between the C1′ atoms (Fig. 3A) of the nucleotides forming the C·C$^+$ base pairs in the first (C^+_1–C^+_3) and third (C_{13}–C_{15}) C-tract, and the second (C_7–C_9) and fourth (C^+_{19}–C^+_{21}) C-tracts of the i-motif structure (Fig. 3B). We calculated the twist angles between C1′ atoms at positions one and three, seven and nine, 13 and 15, and 19 and 21 relative to this axis (Fig. 3C). In the absence of PEGs, the twist angles of C^+_1–C^+_3 and C_{13}–C_{15} were mainly distributed between 20° and 40°, while those of C_7–C_9 were 10°–60° and those of C^+_{19}–C^+_{21} were 10°–40° (Fig. 3D). In the presence of 0.1 M EG_4, C^+_1–C^+_3 showed a wider range of twist angles from 10° to 50°, with a 20° peak as illustrated in the scheme shown in Fig. 3D (orange arrows). These results indicated that EG_4 induced larger fluctuations in the i-motif than in the absence of PEG. However, for EG_9, EG_{13}, and EG_{22}, the twist angle distributions of C^+_1–C^+_3 and C_7–C_9 were narrower than those in the absence of OEG and the presence of EG_4 as illustrated in Fig. 3D (yellow arrows). This suggested that a twisted configuration was restricted in solutions containing large OEGs and PEGs. To highlight the distribution in Fig. 3D, box-and-whisker plots of the twist angles were presented (Supplementary Fig. S12). We also performed MD simulation on the structure of the ILPR i-motif that was recently solved by X-ray crystallography, as well as on another intramolecular i-motif available in the Protein Data Bank [17]. As shown in Supplementary Figs S13 and S14, we analysed the distribution of twist angles in the ILPR iM and observed a slightly broader angle at C^+_4–C^+_7 under PEG200 conditions compared with that in the absence of PEG or in the presence of larger PEGs, as observed in the hTelo iM case. However, the fluctuation in twist angles was smaller than that in the hTelo iM case because the ILPR reference structure was derived from a molecularly packed crystal condition that affected the tetraplex structure compared to the solution conditions. These findings confirmed that the twisting action of the i-motifs, triggered in a size-dependent manner by added PEGs, also occurred in the ILPR iM.

The twisting of i-motif strands might be due to the interaction between the phosphate backbone and counter-ions, because the histogram of the simulated diffusion constant of Na^+ ions showed that >80% of the fraction of Na^+ ions had $<10 \times 10^{-5}$ cm^2 s^{-1} for the diffusion constant, and those fractions in the presence of EG_9 and larger cosolutes were relatively large when compared to in the absence of cosolute or the presence of EG_4 (Supplementary Fig. S15). In the EG_4 condition, the interaction of Na^+ ions with phosphates on the backbone frequently induced changes in the orientation of the strand. By contrast, in the presence of EG_9 and larger ones, the total amount of hydrated water and cations was reduced compared to that in the dilute solutions. This resulted in the restriction of the movement of cations near the backbone for a long time, possibly affecting the twist angle. Therefore, the twisting of the tetraplex orientation could only occur in the presence of PEG400 and the PEGs with larger MWs or EG_6 and the OEGs with larger MWs. However, untwisting might have occurred in the presence of PEG200 or smaller OEGs than EG_6. Thus, putting together the NMR data and results of MD simulation, the twisting of the strands of the i-motif occurred depending on the size of PEGs and OEGs can be one of the factors for stabilization of i-motifs.

Validation of the stability prediction of hTelo iM based on water activity, excluded volume, and twisting of the strand

We tested whether the stability of hTelo iM could be predicted by parameterizing water activity and the excluded volume effect together with the twisting of the i-motif structure. We have recently reported that the duplex stability could be calculated as a sum of the functions including the difference of water activity Δa_w and the unit number of monomers in the cosolute, which were separately calculated the energetic contribution from the propagating the nearest-neighbour (NN) base pairs to form the helix [53]. Following the NN model, the Gibbs free energy change (ΔG°) of the formation of hTelo iM in a certain crowding condition can be led by sum of the stability in the non-crowding condition and the energetical contribution by solution properties as Equation 4.

$$\Delta G^\circ_{37,\mathrm{hteloIM}} = \Delta G^\circ_{37,\mathrm{b-hteloIM}} + \Delta G^\circ_{37,\mathrm{cat-hteloIM}} + \Delta G^\circ_{37,\mathrm{cro-hteloIM}}, \quad (4)$$

where the individual contributions of the bulk interactions ($\Delta G^\circ_{\mathrm{b\text{-}hteloIM}}$) and environmental factors comprise the energetic contribution of the cation ($\Delta G^\circ_{\mathrm{cat\text{-}hteloIM}}$) and crowder ($\Delta G^\circ_{\mathrm{cro\text{-}hteloIM}}$) for the formation of hTelo iM at 37°C. As demonstrated in this study, where the cation concentration is fixed, the sum of the first and second term $\Delta G^\circ_{37,\mathrm{b\text{-}hteloIM}}$ + $\Delta G^\circ_{37,\mathrm{cat\text{-}hteloIM}}$ is equal to ΔG° of the formation of hTelo iM in the non-crowding condition without cosolute at 37°C, that is, $\Delta G^\circ_{37,\mathrm{hteloIM,nc}}$ shown in Equation (5).

$$\Delta G^\circ_{37,\mathrm{hteloIM}} = \Delta G^\circ_{37,\mathrm{hTeloIM,nc}} + \Delta G^\circ_{37,\mathrm{cro-hteloIM}}, \quad (5)$$

The energetic contribution of crowder could be considered as the sum of the individual contributions from the excluded volume effect and water activity [53]. Thus, Equation (5) can be described as presented in Equation (6).

$$\Delta G^\circ_{37,\mathrm{hTeloIM}} = \Delta G^\circ_{37,\mathrm{hTeloIM,nc}} + \Delta G^\circ_{37,\mathrm{ev-hTeloIM}} + \Delta G^\circ_{37,\mathrm{wa-hTeloIM}}, \quad (6)$$

$\Delta G^\circ_{37,\mathrm{ev\text{-}hTeloIM}}$ for the different PEGs and OEGs were then calculated as previous reports [48] (see the materials and

Downloaded from https://academic.oup.com/nar/article/53/12/gkaf500/8178390 by Kemijski Institut user on 16 July 2025

methods in detail) and the values are listed in Supplementary Tables S3 and S4. As for the contribution of the water activity, we reported that $\Delta G^{\circ}_{37,\text{wa-hTeloIM}}$ has a proportional relation with changes in water activity (Δa_w) [53]. Replacing the proportional relation for $\Delta G^{\circ}_{37,\text{ev-hTeloIM}}$ and $\Delta G^{\circ}_{37,\text{wa-hTeloIM}}$ in Equation (6), $\Delta G^{\circ}_{37,\text{hteloIM}}$ is obtained through Equation (7).

$$\Delta G^{\circ}_{37,\text{hTeloIM}} = \Delta G^{\circ}_{37,\text{hTeloIM,nc}} + \left(\Delta G^{\circ}_{37,\text{ev-hTeloIM}} + m_1 \times \Delta a_w\right), \quad (7)$$

where m_1 is a prefactor for cosolutes, equivalent to the energy (kcal mol^{-1}) for the i-motif in the presence of a cosolute, and Δa_w is the value of change in water activity ($a_{\text{cosolute}} - a_{\text{no cosolute}}$). Here, we further introduced another factor, D, about the energetic contribution by the twisted structure in addition to $\Delta G^{\circ}_{37,\text{hTeloIM}}$. As a quantitative index of the dynamics, we used the twist angle for the magnitude of the dynamics of the hTelo iM structure obtained by the MD simulations. The D value is the weight of the structural dynamics of the hTelo iM obtained from the relative value of interquartile range of the averaged all twist angles of the C·C$^+$ base pairs when compared to that without cosolute, as shown in the box-and-whisker plot calculated by the MD simulations (Supplementary Fig. S11 and Supplementary Table S5). By considering the structural factor (D), ΔG° of the twisted form of hTelo iM ($\Delta G^{\circ}_{37,\text{hTeloIM+tw}}$) can be expressed as Equation (8):

$$\Delta G^{\circ}_{37,\text{hTeloIM+tw}} = \Delta G^{\circ}_{37,\text{hTeloIM,nc}} + \left(\Delta G^{\circ}_{37,\text{ev-hTeloIM}} + m_1 \times \Delta a_w\right) + m_2 \times \text{D}, \quad (8)$$

where m_2 is a prefactor for cosolutes, which is equivalent to the value in dimension of kcal mol^{-1} for the i-motif in the presence of each PEG or OEG and D is a dimensionless value as explained above.

When the prefactors of m_1 and m_2 were obtained as -54.5 and 0.33 by the linear least square fitting using a Python program [57], respectively, the $-\Delta G^{\circ}_{37,\text{hTeloIM+tw}}$ values in each crowding condition could be predicted with errors of 6.0% (Supplementary Table S6) which showed better prediction than that without consideration of the D value and has comparable accuracy with the prediction for the stability of the duplexes [58, 59]. This validation indicates that the consideration of the structural properties of the i-motif in addition to the solution properties was required for accurate stability prediction of the i-motifs. On the other hand, the biological impact of the twisting of the i-motif can be affected by not only stability but also dynamics of the structure. Thus, the twisting of the structure may affect the dynamics of i-motif for the reaction along the DNA more than the stability of i-motif.

Biological impact of twisting of i-motif

For biological impact of the dynamics of i-motif structure, we investigated the twisting effect of the i-motif structure on the replication of a DNA strand containing i-motif sequences as i-motif formation may trigger genomic instability [12]. The processive reaction of a DNA polymerase is stalled by the formed i-motif until the i-motif is unfolded [12]. This unfolding process consists of multiple steps including the polymerase binding to the i-motif, induction of a conformational change of i-motif structure, dissociation of the tetraplex structure, and so on. Although the polymerase reaction should be slower than the twisting reaction estimated in the order of microseconds or less from NMR and MD simulation data, the formation of the protein complex with the DNA can be affected, because the dynamics changes of the DNA causes the changes in mobility and direction of motion that perturbs the recognition of the DNA by the protein [60]. If the twisting dynamics triggered by molecular crowding increases or decreases the energetic barrier of the recognition of the i-motif by the polymerase, the following unfolding process of the i-motif induced by the polymerase would be regulated. Here, we tested the DNA polymerase assay using template DNAs with different i-motifs of human genes from ILPR, Bcl2, and Hif1a (named cILPR, cBcl2, and cHif1a) at pH 6.0, with 20 wt% PEGs of different MWs (Supplementary Fig. S16). To examine replication efficiencies with thermodynamics of i-motifs, we analysed the rate constant (k_s) to overcome the replication stall at 37°C and thermodynamic stability ($-\Delta G^{\circ}_{37}$) (Supplementary Figs. S17 and S18) for our original method, called the quantitative study of topology-dependent replication [12, 61 ,62]. This approach can clarify the stability phase diagram of non-canonical structures versus the activation energy of replication process from the polymerase binding to the unfolding the of structure ($\Delta G^{\ddagger}_{37}$). In the analysis, the trend of regression line on the plots of $-\Delta G^{\circ}_{37}$ and $\ln k_s$ suggested that the mechanism of the unfolding of i-motifs by polymerase was common in each case. Figure 4A shows the plots of $-\Delta G^{\circ}_{37}$ and $\ln k_s$ of each i-motif in the presence of PEGs. We reported previously that PEG1000 exhibited replication stalling more strongly than PEG200 [12]. Together with these data, the results obtained from the replication in the presence of the different PEGs indicated that PEG400 and larger PEGs showed a much more efficient replication stall than PEG200 (Fig. 4A). This suggests that twisting and untwisting of the i-motif depending on PEGs affected the efficiency of the replication stall. To quantitatively compare this with each replication kinetics, we introduced α value calculated by $\Delta \ln k_s / \Delta(-\Delta G^{\circ}_{37})$ compared with the data from the reference DNA template not having any secondary structures [12] and determined α values as -0.79 (20 wt% PEG200), -1.7 (20 wt% PEG400), -1.8 (20 wt% PEG600), and -1.6 (20 wt% PEG1000), respectively (Fig. 4B). As $\Delta \ln k_s$ is proportional to the $\Delta G^{\ddagger}_{37}$ [12, 62], the ratio of the α value corresponded to that of $\Delta G^{\ddagger}_{37}$ for resolving the i-motif by KF exo-. The α value obtained in 20 wt% PEG200 was about half of that obtained in larger PEGs, suggesting that the required activation energy for resolving the twisted i-motif structure in the DNA template by polymerase was two-fold larger than that required for resolving the untwisted structure. As a result, the processivity of DNA polymerase along the template may be faster in the solution of PEG 200 than in PEGs of higher MW. Therefore, these results indicate that the twisting step due to the dynamics of the i-motif is dependent on molecular crowding. This regulated the recognition of the i-motif structure by the polymerase to form the polymerase-DNA complex, resulting in regulation of the replication kinetics of i-motif forming DNA.

We previously showed that the topology of G4s could affect replication efficiency due to the difference in unfolding kinetics depending on those structures [12, 61]. The topology of G4 can be recognized or regulated by protein binding in cells [63]. However, almost no protein binds to i-motif in cells [10]. Thus, the biological impact of i-motif on gene replication and expression is probably regulated by the molecular environment in cells. Interestingly, our previous study

Downloaded from https://academic.oup.com/nar/article/53/12/gkaf500/8178390 by Kemijski Institut user on 16 July 2025

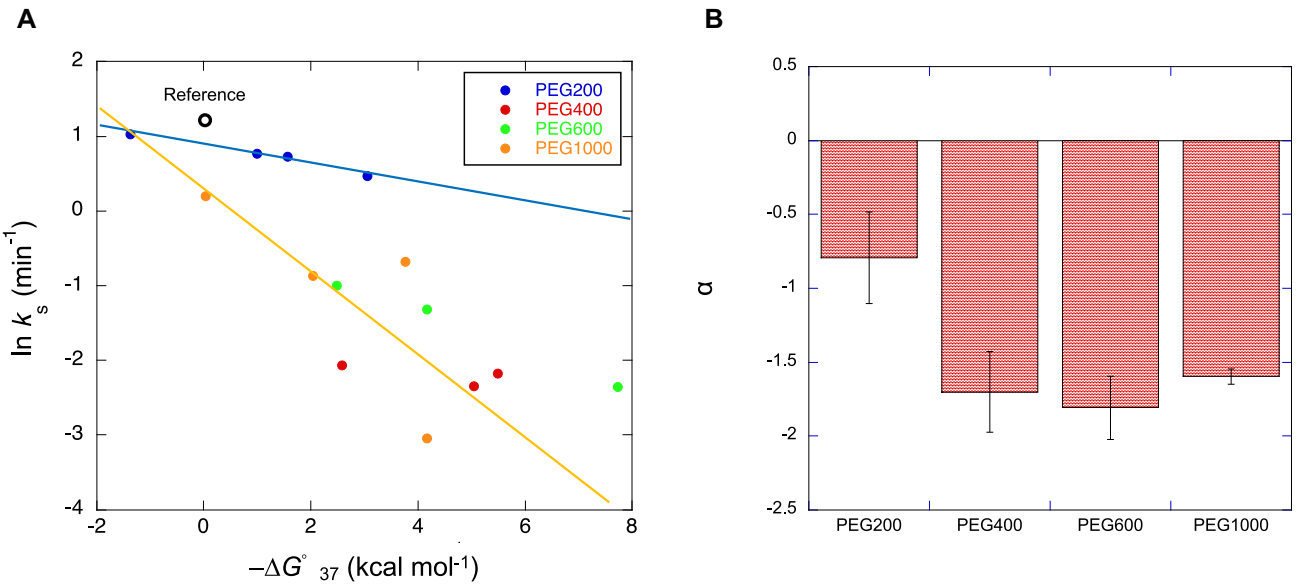

Figure 4. Replication of i-motif containing DNAs affected by twisting with different PEGs. (**A**) Plots for the logarithms of rate constants for reactions versus $-\Delta G^\circ_{37}$ values to produce full-length replication product from i-motif-forming templates in the presence of 20 wt% PEG200 (blue), 20 wt% PEG400 (red), 20 wt% PEG600 (green), and 20 wt% PEG1000 (orange). The blue and orange lines indicate the linear correlation between lnk_s and $-\Delta G^\circ_{37}$ of i-motif-forming sequences in the presence of 20 wt% PEG200 and 20 wt% PEG1000 as reported in our previous study, respectively. [13] All the reactions were performed with 40 mM MES (pH 6.0), 8 mM $MgCl_2$, 100 mM KCl, 20 wt% each PEG, 1 μM KF exo- and 250 μM dNTPs at 37°C. (**B**) Relation between α values and cosolute molecules.

revealed that the environment in the nucleolus of HeLa cells can be mimicked by PEG200 conditions [30]. This suggests that the function of i-motif DNA may be differentially regulated in different areas of the nucleus. As expected, the numbers of foci detected by the i-motif antibody were dynamically changed by cell cycles [6], suggesting changes in the stability and/or the affinity of the antibody to the i-motifs due to the twisting of i-motif induced by the nucleus environment. Particularly, the detection of i-motif was obviously reduced in S-phase of the cell cycle when DNA was replicated [6]. Our results suggest that the molecular environment in cells during S-phase has PEG200 like conditions, reducing the activation energy of the resolving i-motifs for smooth replication. In other words, the disorder of the cellular environment in S-phase can cause the replicative stress, resulting in cancer progression and neurodegenerative diseases [64]. In line with this, it has been reported that i-motif could be an important causal source of genomic instability in cancer cell lines [65]. Therefore, our findings provide an important biological aspect regarding i-motifs, that the stability of the i-motif structures and biological functions of the i-motif in cells can be regulated by twisting the helix by altering cellular environments without binding proteins to i-motifs. Thus, employing i-motif ligands with roles similar to the PEGs could be an attractive strategy for i-motif dependent gene replication and transcription.

Acknowledgements

We thank Ms. J. Inoue and Ms. A. Matsuyama for their assistance with the experiments.

Author contributions: S.T. and N.S. conceived and designed the study; S.T., T.O., and M.T. arranged methods of thermodynamics, NMR-based analyses, MD simulation, and replication assays; S.T., S.G., M.T., and T.O. performed experiments; M.T. and J.P. performed visualization of NMR data; S.T. and T.O. performed visualization of MD simulation data; S.T., S.G., T.O., M.T., and J.P. performed data processing; S.T., J.P., and N.S. supervised research activities; S.T., S.G., T.O., and M.T. wrote the first original draft; all authors contributed to the manuscript review & editing; S.T., J.P., and N.S. secured the research funding.

Supplementary data

Supplementary data is available at NAR online.

Conflict of interest

None declared.

Funding

This work was supported by the Ministry of Education, Culture, Sports, Science, and Technology (MEXT) and the Japan Society for the Promotion of Science (JSPS) (21K05283 and 24K01631), especially for Grant-in-Aid for Scientific Research (S) (22H04975), JSPS Core-to-Core Program (JPJSCCA20220005), JSPS bilateral program (grant no. 120233509), Konan New Century Strategic Research Project, the Asahi Glass Foundation, and the Chubei Itoh Foundation. The authors also acknowledge the CERIC-ERIC consortium for access to experimental facilities (grant no. 20227082). Funding to pay the Open Access publication charges for this article was provided by JSPS. The authors (MT and JP) acknowledge the financial support from Slovenian Research and Innovation Agency [ARIS, grants P1-0242 and J1-60019].

Downloaded from https://academic.oup.com/nar/article/53/12/gkaf500/8178390 by Kemijski Institut user on 16 July 2025

Data availability

All data are available in the main text or Supplementary data.

References

1. Rhodes D, Lipps HJ. G-quadruplexes and their regulatory roles in biology. *Nucleic Acids Res* 2015;**43**:8627–37. https://doi.org/10.1093/nar/gkv862
2. Spiegel J, Balasubramanian S. The Structure and Function of DNA G-Quadruplexes. *Trends Chem* 2020;**2**:123–36. https://doi.org/10.1016/j.trechm.2019.07.002
3. Herbert A. Z-DNA and Z-RNA in human disease. *Commun Biol* 2019;**2**:7. https://doi.org/10.1038/s42003-018-0237-x
4. Varshney D, Spiegel J, Zyner K *et al.* The regulation and functions of DNA and RNA G-quadruplexes. *Nat Rev Mol Cell Biol* 2020;**21**:459–74. https://doi.org/10.1038/s41580-020-0236-x
5. Kiyama R, Camerini-Otero RD. A triplex DNA-binding protein from human cells: purification and characterization. *Proc Natl Acad Sci USA* 1991;**88**:10450–4. https://doi.org/10.1073/pnas.88.23.10450
6. Zeraati M, Langley DB, Schofield P *et al.* I-Motif DNA structures are formed in the nuclei of human cells. *Nat Chem* 2018;**10**:631–7. https://doi.org/10.1038/s41557-018-0046-3
7. Dzatko S, Krafcikova M, Hansel-Hertsch R *et al.* Evaluation of the stability of DNA i-motifs in the nuclei of living mammalian cells. *Angew Chem Int Ed* 2018;**57**:2165–9. https://doi.org/10.1002/anie.201712284
8. King JJ, Irving KL, Evans CW *et al.* DNA G-quadruplex and i-motif structure formation is interdependent in human cells. *J Am Chem Soc* 2020;**142**:20600–4. https://doi.org/10.1021/jacs.0c11708
9. Abou Assi H, Garavis M, Gonzalez C *et al.* i-Motif DNA: structural features and significance to cell biology. *Nucleic Acids Res* 2018;**46**:8038–56. https://doi.org/10.1093/nar/gky735
10. Rogers RA, Fleming AM, Burrows CJ. Rapid screen of potential i-motif forming sequences in DNA repair gene promoters. *ACS Omega* 2018;**3**:9630–5. https://doi.org/10.1021/acsomega.8b01551
11. Dvorakova Z, Renciuk D, Kejnovska I *et al.* i-Motif of cytosine-rich human telomere DNA fragments containing natural base lesions. *Nucleic Acids Res* 2018;**46**:1624–34. https://doi.org/10.1093/nar/gky035
12. Takahashi S, Brazier JA, Sugimoto N. Topological impact of noncanonical DNA structures on Klenow fragment of DNA polymerase. *Proc Natl Acad Sci USA* 2017;**114**:9605–10. https://doi.org/10.1073/pnas.1704258114
13. Kendrick S, Kang HJ, Alam MP *et al.* The dynamic character of the BCL2 promoter i-motif provides a mechanism for modulation of gene expression by compounds that bind selectively to the alternative DNA hairpin structure. *J Am Chem Soc* 2014;**136**:4161–71. https://doi.org/10.1021/ja410934b
14. Miglietta G, Cogoi S, Pedersen EB *et al.* GC-elements controlling HRAS transcription form i-motif structures unfolded by heterogeneous ribonucleoprotein particle A1. *Sci Rep* 2015;**5**:18097. https://doi.org/10.1038/srep18097
15. Kaulage MH, Bhattacharya S, Muniyappa K. Structural characterization of i-motif structure in the human acetyl-CoA carboxylase 1 gene promoters and their role in the regulation of gene expression. *ChemBioChem* 2018;**19**:1078–87. https://doi.org/10.1002/cbic.201800021
16. Takahashi S, Bhattacharjee S, Ghosh S *et al.* Preferential targeting cancer-related i-motif DNAs by the plant flavonol fisetin for theranostics applications. *Sci Rep* 2020;**10**:2504. https://doi.org/10.1038/s41598-020-59343-2
17. Guneri D, Alexandrou E, El Omari K *et al.* Structural insights into i-motif DNA structures in sequences from the insulin-linked polymorphic region. *Nat Commun* 2024;**15**:7119. https://doi.org/10.1038/s41467-024-50553-0
18. El-Khoury R, Roman M, Assi HA *et al.* Telomeric i-motifs and C-strands inhibit parallel G-quadruplex extension by telomerase. *Nucleic Acids Res* 2023;**51**:10395–410. https://doi.org/10.1093/nar/gkad764
19. Martella M, Pichiorri F, Chikhale RV *et al.* i-Motif formation and spontaneous deletions in human cells. *Nucleic Acids Res* 2022;**50**:3445–55. https://doi.org/10.1093/nar/gkac158
20. Kang HJ, Kendrick S, Hecht SM *et al.* The transcriptional complex between the BCL2 i-motif and hnRNP LL is a molecular switch for control of gene expression that can be modulated by small molecules. *J Am Chem Soc* 2014;**136**:4172–85. https://doi.org/10.1021/ja4109352
21. Sutherland C, Cui Y, Mao H *et al.* A mechanosensor mechanism controls the G-quadruplex/i-motif molecular switch in the MYC promoter NHE III1. *J Am Chem Soc* 2016;**138**:14138–51. https://doi.org/10.1021/jacs.6b09196
22. Gao B, Zheng YT, Su AM *et al.* Remodeling the conformational dynamics of I-motif DNA by helicases in ATP-independent mode at acidic environment. *iScience* 2022;**25**:103575. https://doi.org/10.1016/j.isci.2021.103575
23. Ban Y, Ando Y, Terai Y *et al.* Profiling of i-motif-binding proteins reveals functional roles of nucleolin in regulation of high-order DNA structures. *Nucleic Acids Res* 2024;**52**:13530–43. https://doi.org/10.1093/nar/gkae1001
24. Cheng M, Qiu D, Tamon L *et al.* Thermal and pH stabilities of i-DNA: confronting in vitro experiments with models and in-cell NMR data. *Angew Chem Int Ed* 2021;**60**:10286–94. https://doi.org/10.1002/anie.202016801
25. Zimmerman SB, Trach SO. Estimation of macromolecule concentrations and excluded volume effects for the cytoplasm of *Escherichia coli*. *J Mol Biol* 1991;**222**:599–620. https://doi.org/10.1016/0022-2836(91)90499-V
26. Minton AP. Quantitative assessment of the relative contributions of steric repulsion and chemical interactions to macromolecular crowding. *Biopolymers* 2013;**99**:239–44. https://doi.org/10.1002/bip.22163
27. Nakano S, Miyoshi D, Sugimoto N. Effects of molecular crowding on the structures, interactions, and functions of nucleic acids. *Chem Rev* 2014;**114**:2733–58. https://doi.org/10.1021/cr400113m
28. Takahashi S, Sugimoto N. Stability prediction of canonical and non-canonical structures of nucleic acids in various molecular environments and cells. *Chem Soc Rev* 2020;**49**:8439–68. https://doi.org/10.1039/D0CS00594K
29. Cheng M, Chen J, Ju H *et al.* Drivers of i-DNA formation in a variety of environments revealed by four-dimensional UV melting and annealing. *J Am Chem Soc* 2021;**143**:7792–807. https://doi.org/10.1021/jacs.1c02209
30. Takahashi S, Yamamoto J, Kitamura A *et al.* Characterization of intracellular crowding environments with topology-based DNA quadruplex sensors. *Anal Chem* 2019;**91**:2586–90. https://doi.org/10.1021/acs.analchem.8b04177
31. Nott TJ, Craggs TD, Baldwin AJ. Membraneless organelles can melt nucleic acid duplexes and act as biomolecular filters. *Nat Chem* 2016;**8**:569–75. https://doi.org/10.1038/nchem.2519
32. Gao M, Gnutt D, Orban A *et al.* RNA hairpin folding in the crowded cell. *Angew Chem Int Ed* 2016;**55**:3224–8. https://doi.org/10.1002/anie.201510847
33. Rajendran A, Nakano S-i, Sugimoto N. Molecular crowding of the cosolutes induces an intramolecular i-motif structure of triplet repeat DNA oligomers at neutral pH. *Chem Commun* 2010;**46**:1299–301. https://doi.org/10.1039/b922050j
34. Liu L, Kim BG, Feroze U *et al.* Probing the ionic atmosphere and hydration of the c-MYC i-motif. *J Am Chem Soc* 2018;**140**:2229–38. https://doi.org/10.1021/jacs.7b11537
35. Zanin I, Ruggiero E, Nicoletto G *et al.* Genome-wide mapping of i-motifs reveals their association with transcription regulation in live human cells. *Nucleic Acids Res* 2023;**51**:8309–21. https://doi.org/10.1093/nar/gkad626

Downloaded from https://academic.oup.com/nar/article/53/12/gkaf500/8178390 by Kemijski Institut user on 16 July 2025

36. Tateishi-Karimata H, Nakano SI, Sugimoto N. Quantitative analyses of nucleic acid stability under the molecular crowding condition induced by cosolutes. *Curr Protoc Nucleic Acid Chem* 2013;**53**:7.19.1-7.19.17. https://doi.org/10.1002/0471142700.nc0719s53
37. Matsumoto S, Takahashi S, Bhowmik S *et al.* Volumetric strategy for quantitatively elucidating a local hydration network around a G-quadruplex. *Anal Chem* 2022;**94**:7400–7. https://doi.org/10.1021/acs.analchem.2c01075
38. Takahashi S, Okura H, Chilka P *et al.* Molecular crowding induces primer extension by RNA polymerase through base stacking beyond Watson–Crick rules. *RSC Adv* 2020;**10**:33052–8. https://doi.org/10.1039/D0RA06502A
39. Lee W, Tonelli M, Markley JL. NMRFAM-SPARKY: enhanced software for biomolecular NMR spectroscopy. *Bioinformatics* 2015;**31**:1325–7. https://doi.org/10.1093/bioinformatics/btu830
40. Phan AT, Gueron M, Leroy JL. The solution structure and internal motions of a fragment of the cytidine-rich strand of the human telomere. *J Mol Biol* 2000;**299**:123–44. https://doi.org/10.1006/jmbi.2000.3613
41. Pérez A, Marchán I, Svozil D *et al.* Refinement of the AMBER force field for nucleic acids: improving the description of α/γ conformers. *Biophys J* 2007;**92**:3817–29. https://doi.org/10.1529/biophysj.106.097782
42. Wang J, Wolf RM, Caldwell JW *et al.* Development and testing of a general amber force field. *J Comput Chem* 2004;**25**:1157–74. https://doi.org/10.1002/jcc.20035
43. Wang J, Wang W, Kollman PA *et al.* Automatic atom type and bond type perception in molecular mechanical calculations. *J Mol Graph Model* 2006;**25**:247–60. https://doi.org/10.1016/j.jmgm.2005.12.005
44. Frisch MJ *et al.* . Gaussian 09Rev. D.01. USA: Wallingford, 2016. https://gaussian.com/g09citation/
45. Sousa da Silva AW, Vranken WF. ACPYPE—AnteChamber PYthon Parser interfacE. *BMC Res Notes* 2012;**5**:367. https://doi.org/10.1186/1756-0500-5-367
46. Abraham MJ, Murtola T, Schulz R *et al.* GROMACS: high performance molecular simulations through multi-level parallelism from laptops to supercomputers. *SoftwareX* 2015;**1–2**:19–25. https://doi.org/10.1016/j.softx.2015.06.001
47. Jorgensen WL, Chandrasekhar J, Madura JD *et al.* Comparison of simple potential functions for simulating liquid water. *J Chem Phys* 1983;**79**:926–35. https://doi.org/10.1063/1.445869
48. Knowles DB, LaCroix AS, Deines NF *et al.* Separation of preferential interaction and excluded volume effects on DNA duplex and hairpin stability. *Proc Natl Acad Sci USA* 2011;**108**:12699–704. https://doi.org/10.1073/pnas.1103382108
49. Hermans J. Excluded-volume theory of polymer–protein interactions based on polymer chain statistics. *J Chem Phys* 1982;**77**:2193–203. https://doi.org/10.1063/1.444026
50. Miyoshi D, Nakamura K, Tateishi-Karimata H *et al.* Hydration of Watson–Crick base pairs and dehydration of Hoogsteen base pairs inducing structural polymorphism under molecular crowding conditions. *J Am Chem Soc* 2009;**131**:3522–31. https://doi.org/10.1021/ja805972a
51. Devoe H, Tinoco I Jr. The hypochromism of helical polynucleotides. *J Mol Biol* 1962;**4**:518–27. https://doi.org/10.1016/S0022-2836(62)80106-5
52. Sedghi Masoud S, Yamaoki Y, Ma Y *et al.* Analysis of interactions between Telomeric i-motif DNA and a cyclic tetraoxazole compound. *ChemBioChem* 2018;**19**:2268–72. https://doi.org/10.1002/cbic.201800425
53. Ghosh S, Takahashi S, Banerjee D *et al.* Nearest-neighbor parameters for the prediction of RNA duplex stability in diverse in vitro and cellular-like crowding conditions. *Nucleic Acids Res* 2023;**51**:4101–11. https://doi.org/10.1093/nar/gkad020
54. Nakano S, Karimata H, Ohmichi T *et al.* The effect of molecular crowding with nucleotide length and cosolute structure on DNA duplex stability. *J Am Chem Soc* 2004;**126**:14330–1. https://doi.org/10.1021/ja0463029
55. Bhavsar-Jog YP, Van Dornshuld E, Brooks TA *et al.* Epigenetic modification, dehydration, and molecular crowding effects on the thermodynamics of i-motif structure formation from C-rich DNA. *Biochemistry* 2014;**53**:1586–94. https://doi.org/10.1021/bi401523b
56. Mergny J-L, Lacroix L, Han X *et al.* Intramolecular folding of pyrimidine oligodeoxynucleotides into an i-DNA motif. *J Am Chem Soc* 1995;**117**:8887–98. https://doi.org/10.1021/ja00140a001
57. Ghosh S, Takahashi S, Endoh T *et al.* Validation of the nearest-neighbor model for Watson–Crick self-complementary DNA duplexes in molecular crowding condition. *Nucleic Acids Res* 2019;**47**:3284–94. https://doi.org/10.1093/nar/gkz071
58. Adams MS, Znosko BM. Thermodynamic characterization and nearest neighbor parameters for RNA duplexes under molecular crowding conditions. *Nucleic Acids Res* 2019;**47**:3658–66. https://doi.org/10.1093/nar/gkz019
59. Xia T, SantaLucia J Jr., Burkard ME *et al.* Thermodynamic parameters for an expanded nearest-neighbor model for formation of RNA duplexes with Watson–Crick base pairs. *Biochemistry* 1998;**37**:14719–35. https://doi.org/10.1021/bi9809425
60. Pederson K, Meints GA, Drobny GP. Base dynamics in the HhaI protein binding site. *J Phys Chem B* 2023;**127**:7266–75. https://doi.org/10.1021/acs.jpcb.3c03687
61. Takahashi S, Kim KT, Podbevsek P *et al.* Recovery of the formation and function of oxidized G-quadruplexes by a pyrene-modified guanine tract. *J Am Chem Soc* 2018;**140**:5774–83. https://doi.org/10.1021/jacs.8b01577
62. Takahashi S, Kotar A, Tateishi-Karimata H *et al.* Chemical modulation of DNA replication along G-quadruplex based on topology-dependent ligand binding. *J Am Chem Soc* 2021;**143**:16458–69. https://doi.org/10.1021/jacs.1c05468
63. Zaug AJ, Podell ER, Cech TR. Human POT1 disrupts telomeric G-quadruplexes allowing telomerase extension in vitro. *Proc Natl Acad Sci USA* 2005;**102**:10864–9. https://doi.org/10.1073/pnas.0504744102
64. Maizels N. G4-associated human diseases. *EMBO Rep* 2015;**16**:910–22. https://doi.org/10.15252/embr.201540607
65. Amparo C, Clark J, Bedell V *et al.* Duplex DNA from sites of helicase-polymerase uncoupling links non-B DNA structure formation to replicative stress. *Cancer Genomics Proteomics* 2020;**17**:101–15. https://doi.org/10.21873/cgp.20171

Received: December 17, 2024. **Revised:** April 14, 2025. **Editorial Decision:** May 1, 2025. **Accepted:** June 18, 2025
© The Author(s) 2025. Published by Oxford University Press on behalf of Nucleic Acids Research.
This is an Open Access article distributed under the terms of the Creative Commons Attribution-NonCommercial License (https://creativecommons.org/licenses/by-nc/4.0/), which permits non-commercial re-use, distribution, and reproduction in any medium, provided the original work is properly cited. For commercial re-use, please contact reprints@oup.com for reprints and translation rights for reprints. All other permissions can be obtained through our RightsLink service via the Permissions link on the article page on our site—for further information please contact journals.permissions@oup.com.

Downloaded from https://academic.oup.com/nar/article/53/12/gkaf500/8178390 by Kemijski Institut user on 16 July 2025